Letter

# Maximized $K/J$ ratio and cubiclike $j_{\text{eff}} = \frac{1}{2}$ moments in a noncubic environment in $\alpha$-$RuCl_3$ under pressure

Pritam Bhattacharyya,[1] Liviu Hozoi,[1] Satoshi Nishimoto,[1,2] Quirin Stahl,[3] Jochen Geck,[3,4] and Nikolay A. Bogdanov[5]

[1]*Institute for Theoretical Solid State Physics, Leibniz IFW Dresden, Helmholtzstraße 20, 01069 Dresden, Germany*

[2]*Department of Physics, Technical University Dresden, 01069 Dresden, Germany*

[3]*Institut für Festkörper- und Materialphysik, Technische Universität Dresden, 01062 Dresden, Germany*

[4]*Würzburg-Dresden Cluster of Excellence ct.qmat, Technische Universität Dresden, 01062 Dresden, Germany*

[5]*Max Planck Institute for Solid State Research, Heisenbergstraße 1, 70569 Stuttgart, Germany*

(Received 1 February 2023; revised 20 June 2023; accepted 4 October 2023; published 23 October 2023)

Maximization of the ratio between Kitaev and residual Heisenberg interactions is a major goal in the current research on Kitaev-Heisenberg magnets. Here we investigate Kitaev-Heisenberg exchange in a recently discovered crystalline phase of $\alpha$-$RuCl_3$ under pressure—it displays unusually high symmetry, with only one type of Ru-Ru links and uniform Ru-Cl-Ru bond angles of $\approx 93^\circ$. Using quantum chemical calculations, we find a very small nearest-neighbor Heisenberg $J$, which yields a $K/J$ ratio between Kitaev and Heisenberg exchange as large as $\sim 100$. We also find that this is associated with vanishingly small $d$-shell trigonal splittings, i.e., minimal departure from ideal $j_{\text{eff}} = 1/2$ moments. This reconfirms $RuCl_3$ as a most promising platform for materializing the much sought-after Kitaev spin-liquid phase and should stimulate further experiments under strain and pressure.

DOI: 10.1103/PhysRevB.108.L161107

*Introduction.* Many magnetic materials can be described as extended collections of atomic magnetic moments. Electronic correlations, along with relativistic effects and specific crystallographic features, determine (i) the character of those moments and (ii) how they interact with each other. Magnetic moments are parametrized in terms of (pseudo)spin quantum numbers and $g$ factors; their interaction is through effective coupling constants (ECCs). The latter may imply isotropic terms (defining Heisenberg's textbook model of interacting moments), but also anisotropic contributions, symmetric and/or antisymmetric; in other words, several effective interaction parameters. The anisotropic ECCs were long regarded as just small perturbations to the isotropic terms; yet, it now appears that in certain magnets, they actually define the largest interaction scale. Small perturbation turned into dominant interaction obviously represents a radical change of frame, i.e., a change of paradigm, in magnetism research.

Research in this area has recently boomed with the realization that large anisotropic ECCs may give rise to novel, exotic magnetic phases, e.g., peculiar flavors of quantum spin liquids (QSLs). The latter represent special states of matter that display quantum entanglement and can host unconventional fractionalized excitations. Such properties are of genuine fundamental interest; they may also have far-reaching implications and a decisive impact on technology, e.g., data storage, memory devices, and (topological) quantum computation, if suitable QSL materials are identified. Special attention is presently being paid to honeycomb, but also triangular magnetic lattices. A main driving force is Kitaev's concept of bond-dependent anisotropic interactions on a honeycomb network of localized moments [1]. Sizable, bond-dependent Kitaev interactions [1,2] have now been confirmed in several honeycomb transition-metal oxides and halides. The magnetic ground state, however, is, in most of these systems, ordered due to residual isotropic Heisenberg couplings, involving both nearest [3,4] and farther neighbors. A main question is therefore which the most suited chemical platforms and set of structural parameters are (e.g., bond lengths and bond angles) that maximize the ratio between Kitaev and Heisenberg exchange.

A distinct system in this context is $\alpha$-$RuCl_3$: although it is ordered antiferromagnetically under normal conditions, this antiferromagnetic phase lies in close proximity to a QSL state [6]. The latter can be reached by applying a modest in-plane magnetic field [7–9], which raises the question of whether strain or pressure could be used as well for tuning the magnetic ground state. Interestingly, a new crystalline phase has recently been identified under a pressure of 1.26 GPa [5]; see Fig. 1. Here we report *ab initio* quantum chemical results for the Ru-site multiplet structure and nearest-neighbor ECCs in this recently discovered crystalline arrangement. The computations reveal an unusually large $K/J$ ratio of $\sim 100$ between Kitaev ($K$) and Heisenberg ($J$) ECCs, reconfirming $\alpha$-$RuCl_3$ as one of the most promising chemical settings for materializing the Kitaev QSL ground state. Additionally, we find a very peculiar inner structure of the effective moments, with $d$-shell trigonal crystal-field splittings as low as 9 meV, which is 4–5 times less than in $\alpha$-$RuCl_3$ under ambient pressure [10–13]. This points to minimal departure from ideal $j_{\text{eff}} = 1/2$ moments [2,14], through near cancellation of two different effects—trigonal compression of the ligand cage and anisotropic fields related to farther ions. The apparent correlation between minimal departure from ideal, cubic-symmetry $j_{\text{eff}} = 1/2$ moments and maximized $K/J$ ratio is quite

 

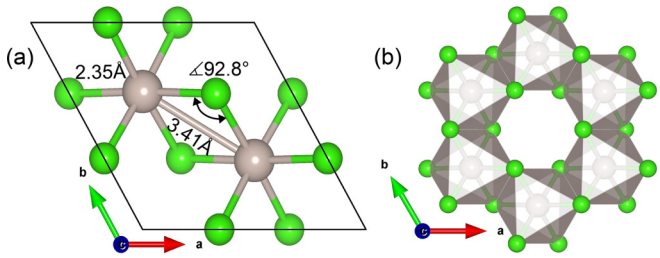


FIG. 1. (a) Unit cell of $\alpha$-$RuCl_3$ for $p = 1.26$ GPa [5]. (b) Hexagonal ring of edge-sharing $RuCl_6$ octahedra. Gray and green spheres represent Ru and Cl ions, respectively.

remarkable. It seems to indicate that the nearest-neighbor $J$ is minimized in the case of degenerate $t_{2g}$ orbitals.

*Ru-site multiplet structure, nature of magnetic moments.* The electrostatic field due to the ligand ions around each ruthenium magnetic center splits the valence Ru $4d$ levels into $e_g$ and $t_{2g}$ components, with the latter lying at significantly lower energy; the large $t_{2g}$–$e_g$ splitting then yields a $t_{2g}^5$ leading ground-state configuration. With one hole ($s = 1/2$) in the $t_{2g}$ sector ($l_{\text{eff}} = 1$), sizable spin-orbit coupling (SOC) provides a set of fully occupied $j_{\text{eff}} = 3/2$ and magnetically active $j_{\text{eff}} = 1/2$ states [2,14]. For threefold [5] (or lower) site symmetry, the degeneracy of the $t_{2g}$ sublevels is typically lifted and the $j_{\text{eff}} = 1/2$ and $j_{\text{eff}} = 3/2$ spin-orbit states may feature some degree of admixture.

To determine the $Ru^{3+}$ $4d^5$ multiplet structure in $\alpha$-$RuCl_3$ at $p = 1.26$ GPa, we carried out quantum chemical computations using the MOLPRO suite of programs [15] and crystallographic data as reported by Stahl *et al.* [5]. A cluster consisting of one "central" $RuCl_6$ octahedron and the three in-plane adjacent octahedra was designed for this purpose (see Supplemental Material [16]). The crystalline environment was modeled as a large array of point charges which reproduces the Madelung field within the cluster volume; to generate this point-charge embedding, we employed the EWALD program [17,18]. The numerical investigation was initiated as a complete active space self-consistent field (CASSCF) calculation [19,20] with all five $4d$ orbitals of the central Ru ion considered in the active orbital space. Post-CASSCF correlation computations were carried out at the level of multireference configuration interaction (MRCI) with single and double excitations [19,21] out of the Ru $4d$ and Cl $3p$ orbitals of the central $RuCl_6$ octahedron. SOCs were accounted for following the procedure described in Ref. [22].

The $Ru^{3+}$ $4d^5$ multiplet structure in the newly discovered crystalline phase of $\alpha$-$RuCl_3$ is depicted in Table I, at three different levels of approximation: CASSCF, MRCI, and MRCI + SOC. This allows one to easily disentangle three different effects: crystal-field splittings, post-CASSCF correlation-induced corrections, and spin-orbit interactions. As concerns the former, we find that the trigonal splitting within the $t_{2g}$ levels is tiny, i.e., 9 meV, which is 4–5 times smaller than in $\alpha$-$RuCl_3$ at ambient pressure [10–13]. Having nearly degenerate $t_{2g}$ levels for a sizable amount of trigonal distortion of the ligand cage sounds odd at first. What makes it happen is the presence of a competing effect—trigonal fields related to the anisotropy of the extended solid-state environment. Remarkably, mutual (near) cancellation of those two yields a cubiclike Ru-site multiplet structure. Also quite evident in Table I is the presence of minimal splittings within the $j_{\text{eff}} = 3/2$-like manifold once SOC is accounted for (last column), i.e., minimal admixture among the $j_{\text{eff}} = 1/2$ and $j_{\text{eff}} = 3/2$ spin-orbit states. It is additionally seen that the post-CASSCF MRCI treatment yields sizable corrections to some of the relative energies, the most substantial arising for the $^6A_{1g}$ crystal-field term.

TABLE I. $Ru^{3+}$ $4d^5$ multiplet structure. Each value in the MRCI+SOC column indicates a Kramers doublet (KD); for each of the $t_{2g}^4 e_g^1$ crystal-field terms, only the lowest and highest KDs are shown. Only the crystal-field terms enlisted in the table were included in the spin-orbit computation. Notations corresponding to $O_h$ symmetry are used.

| $Ru^{3+}$ $4d^5$ splittings (eV) | CASSCF | MRCI | MRCI +SOC |
|---|---|---|---|
| $^2T_{2g}$ $(t_{2g}^5)$ | 0 | 0 | 0 |
| | 0.01 | 0.01 | 0.19 |
| | 0.01 | 0.01 | 0.20 |
| $^4T_{1g}$ $(t_{2g}^4 e_g^1)$ | 1.16 | 1.32 | 1.38 |
| | 1.17 | 1.32 | \| |
| | 1.17 | 1.32 | 1.49 |
| $^6A_{1g}$ $(t_{2g}^3 e_g^2)$ | 1.15 | 1.59 | 1.78 (×3) |
| $^4T_{2g}$ $(t_{2g}^4 e_g^1)$ | 1.84 | 1.93 | 2.06 |
| | 1.85 | 1.94 | \| |
| | 1.85 | 1.94 | 2.11 |

*Intersite magnetic couplings for proximate $j_{\text{eff}} = 1/2$ moments.* To obtain the intersite effective magnetic couplings, calculations for a block of two edge-sharing $RuCl_6$ octahedra were performed. The four in-plane octahedra coordinating this two-octahedra central unit were also explicitly included in the quantum chemical computations, but using more compact basis sets (see Supplemental Material [16] for detailed information). The farther solid-state surroundings were also in this case modeled through Madelung-field point-charge embedding [17,18]. CASSCF computations were carried out with six (Ru $t_{2g}$) valence orbitals and 10 electrons as active [abbreviated as (10e,6o) active space]. In the subsequent MRCI treatment, single and double excitations out of the central-unit Ru $t_{2g}$ and bridging-Cl $3p$ orbitals were accounted for. The initial CASSCF optimization was performed for the lowest nine singlet and lowest nine triplet states associated with the (10e,6o) setting. Those were the states for which SOCs were further accounted for [22], either at the CASSCF or MRCI level, which yields, in each case, a number of 36 spin-orbit states.

Only one type of Ru-Ru link is present in $\alpha$-$RuCl_3$ at $p = 1.26$ GPa. A unit of two nearest-neighbor octahedra exhibits $C_{2h}$ point-group symmetry, implying a generalized bilinear effective spin Hamiltonian of the following form for a pair of adjacent 1/2-pseudospins $\tilde{\mathbf{S}}_i$ and $\tilde{\mathbf{S}}_j$:

$$\mathcal{H}_{ij}^{(\gamma)} = J\tilde{\mathbf{S}}_i \cdot \tilde{\mathbf{S}}_j + K\tilde{S}_i^{\gamma}\tilde{S}_j^{\gamma} + \sum_{\alpha\neq\beta}\Gamma_{\alpha\beta}\,(\tilde{S}_i^{\alpha}\tilde{S}_j^{\beta} + \tilde{S}_i^{\beta}\tilde{S}_j^{\alpha}). \quad (1)$$

The $\Gamma_{\alpha\beta}$ coefficients denote the off-diagonal components of the $3 \times 3$ symmetric-anisotropy exchange tensor, with $\alpha, \beta, \gamma \in \{x, y, z\}$. An antisymmetric Dzyaloshinskii-Moriya coupling is not allowed, given the inversion center. The lowest four spin-orbit eigenstates from the *ab initio* quantum chemical output (eigenvalues lower by ∼0.2 eV with respect to the eigenvalues of higher-lying excited states, as illustrated, for example, in Table I) are mapped for each different set of calculations onto the eigenvectors of the effective spin Hamiltonian (1), following the procedure described in Refs. [10,23]: those four expectation values and the matrix elements of the Zeeman Hamiltonian in the basis of the four lowest-energy spin-orbit eigenvectors are put in direct correspondence with the respective eigenvalues and matrix elements of (1). Having two of the states in the same irreducible representation of the $C_{2h}$ point group, such a one-to-one mapping translates into two possible sets of effective magnetic couplings. The relevant array is chosen as the one whose $g$ factors fit the $g$ factors corresponding to a single $RuCl_6$ $t_{2g}^5$ octahedron. We used the standard coordinate frame usually employed in the literature, different from the rotated frame employed in earlier quantum chemical studies [10,24] that affects the sign of $\Gamma$ (see, also, discussion in Ref. [25]).

The nearest-neighbor ECCs obtained by spin-orbit MRCI are $K = -3.73$, $J = -0.03$, $\Gamma \equiv \Gamma_{xy} = 1.62$, and $\Gamma' \equiv \Gamma_{yz} = \Gamma_{zx} = 0.45$ (meV). A remarkable finding is the vanishingly small $J$ value in the MRCI + SOC computations, which yields a fully anisotropic $K$-$\Gamma$-$\Gamma'$ effective spin model for the nearest-neighbor magnetic interactions. That this coincides with realizing nearly ideal $j_{\text{eff}} = 1/2$ moments at the transition-metal sites seems to be more than merely fortuitous, as also discussed in the next section.

The competition between ligand and "crystal" trigonal fields (i.e., between nearest-neighbor and beyond-nearest-neighbor electrostatics) and possible important implications as concerns the overall magnetic properties of a given system have been discussed earlier in relation to single-site effective magnetic parameters such as the single-ion anisotropy [26]—in particular, it is, in principle, possible to revert the sign of the latter by modifying the amount of ligand-cage trigonal distortion [26]. Finding that this applies as well to intersite effective interaction parameters (i.e., the Heisenberg $J$) is even more exciting. For comparison, the MRCI nearest-neighbor couplings in $\alpha$-$RuCl_3$ at ambient pressure are $K = -5.6$, $J = 1.2$, $\Gamma = 1.2$, and $\Gamma' = -0.7$ (meV) [10]. The Heisenberg $J$ being sizable at ambient pressure, the $K/J$ ratio is much smaller [10]. This corresponds to somewhat stronger trigonal compression of the $Cl_6$ polyhedron and additional small distortions that actually lower the Ru-site point-group symmetry to less than trigonal.

*Trigonal splittings in related iridate structures.* Spotting this particular $RuCl_3$ crystalline arrangement, where (i) the effects of ligand-cage trigonal compression and of farther-surrounding trigonal fields cancel out each other, (ii) the Ru-site $t_{2g}$ levels are consequently degenerate (or nearly degenerate), such that close to ideal $j_{\text{eff}} = 1/2$ moments are realized, and (iii) the intersite isotropic Heisenberg interaction approaches zero, raises the question of whether an equivalent sweet spot can be identified in related Kitaev-Heisenberg quantum magnets, e.g., in Ir-oxide honeycomb compounds.

Interestingly, the fact that the Heisenberg $J$ changes its sign and therefore reaches a point where it simply vanishes has already been pointed out, for both "213" hypothetical iridate structures [24] and $H_3LiIr_2O_6$ [27]. Such a situation is achieved in iridates for ligand-cage trigonal squeezing providing Ir-O-Ir bond angles of ≈98° [24,27], but an analysis of the on-site multiplet spectra was not performed in those specific iridate crystalline settings.

To verify this important aspect, we carried out additional quantum chemical computations for "iridate" embedded clusters, i.e., CASSCF calculations for a fragment consisting of one $IrO_6$ octahedron as the central quantum mechanical unit (see Supplemental Material [16] for details). The outcome of this numerical test is rewarding: also in the iridate system, a vanishing Heisenberg $J$ [24] is associated with vanishing $d$-shell trigonal splittings, i.e., a minor deviation from pristine $j_{\text{eff}} = 1/2$ states. In particular, without accounting for SOC, we find a trigonal splitting of only 25 meV within the Ir $t_{2g}$ levels, to be compared with a spin-orbit coupling constant of 400–500 meV for Ir ions. That the near cancellation of ligand and "crystal" trigonal fields occurs for stronger trigonal compression of the ligand cage (≈98° vs ≈93° metal-ligand-metal bond angles) has to do with the larger effective charges in iridium oxides (formally, $Ir^{4+}$ vs $Ru^{3+}$ magnetic sites and $O^{2-}$ vs $Cl^-$ ligands). Notably, various Kitaev-Heisenberg superexchange models do assume (for simplicity) degenerate $t_{2g}$ levels, but not distorted metal-ligand-metal superexchange paths with bond angles away from 90°.

*Phase diagram for $J = 0$ and finite third-neighbor Heisenberg coupling $J_3$.* The magnetic ground state of the extended lattice is, in most Kitaev-Heisenberg honeycomb systems, ordered due to finite isotropic Heisenberg couplings, involving both nearest [3,4] and farther neighbors [10,11]. A natural question is under which conditions the $K/J$ ratio is maximized. A vanishing nearest-neighbor $J$, as found here, is therefore promising. To illustrate the chance of materializing a QSL ground state in $\alpha$-$RuCl_3$ under a pressure of 1.26 GPa, by effective-model exact diagonalization calculations (see Supplemental Material [16] for computational details and additional plots), we derived extended phase diagrams for variable $\Gamma$, $\Gamma'$, and third-neighbor Heisenberg coupling $J_3$, while $J$ is set to 0.

Starting with the case of negligible $J_3$, it is seen in Fig. 2(a) that QSL ground states are found for a wide range of $\Gamma > 0$ and $\Gamma' > 0$ values. The expectation value of the flux operator $W_p = 2^6 S_1^x S_2^y S_3^z S_4^x S_5^y S_6^z$ is illustrated through a color map. The computed QSL phases can be classified into three categories: Kitaev QSL ($\langle W_p \rangle \sim 1$ [1]) near $\Gamma = \Gamma' = 0$, QSL1 with a slow decay of spin-spin correlations due to strong ferromagnetic fluctuations, and QSL2 with a rapid decay of spin-spin correlations, similar to the Kitaev QSL. In the QSL2 region, $\langle W_p \rangle$ is negative but its absolute value is not small, $|\langle W_p \rangle| \sim 0.4$. A typical spin structure factor for the QSL2 phase is shown in the inset of Fig. 2(a). Such a star-shaped structure factor indicates a proximate Kitaev QSL [28] displaying nonvanishing longer range spin-spin correlations. As concerns the ferromagnetic (FM) phase, it resembles a ferrimagnetic state for large $\Gamma$ and $\Gamma'$ values.

A phase diagram computed for variable $\Gamma$ and $J_3$ is provided in Fig. 2(b). The $J_3$ Heisenberg coupling is known to

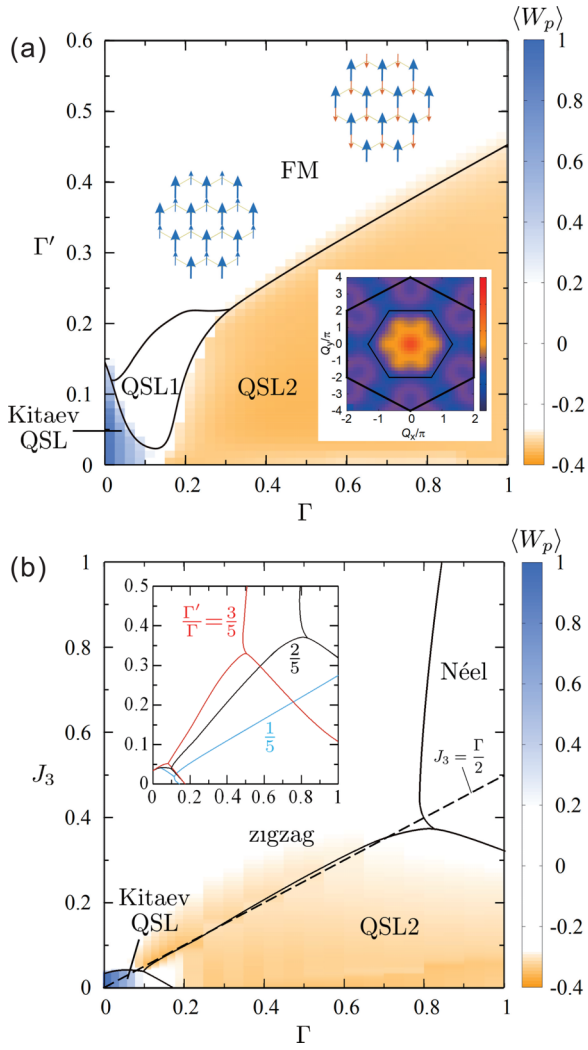


FIG. 2. (a) Generic phase diagram for variable off-diagonal couplings $\Gamma$ and $\Gamma'$ in units of the ferromagnetic Kitaev interaction parameter $|K|$. Inset: spin structure factor illustrating the proximate Kitaev spin liquid [28] in the QSL2 region. (b) Phase diagram for variable $\Gamma$ and third-neighbor Heisenberg coupling $J_3$; $K$ and $\Gamma'/\Gamma$ are set to –1 and 2/5, respectively. Inset: phase boundaries for additional $\Gamma'/\Gamma$ ratios.

be finite and antiferromagnetic in $\alpha$-$RuCl_3$ [11]. The second-neighbor Heisenberg interaction $J_2$, on the other hand, is much weaker and usually neglected [11,29]. Our analysis shows that for $J_3 \lesssim \Gamma/2$, a regime that is confirmed by fits of inelastic neutron scattering spectra [29], the quantum spin liquid is stable, even for $\Gamma'/\Gamma = 0.2$, i.e., a ratio of the two off-diagonal couplings that is significantly smaller than the ratio derived by spin-orbit MRCI.

*Conclusions.* In spite of being a central figure in the current research on quantum magnetism, textbook $j_{\text{eff}} = 1/2$ spin-orbit ground states [14] are rarely found in solids [30–34]. Here we show that nearly ideal $j_{\text{eff}} = 1/2$ moments are realized in a recently reported crystalline phase of $\alpha$-$RuCl_3$, identified under a pressure of 1.26 GPa [5]. In particular, we compute a vanishingly small trigonal splitting within the transition-metal $t_{2g}$ valence subshell in this crystallographic setting. Remarkably, this occurs in the presence of sizable trigonal squeezing of the ligand cages—it turns out that the effect of the latter is counterbalanced by trigonal fields having to do with the more distant crystalline surroundings. Moreover, the nearly ideal $j_{\text{eff}} = 1/2$ character of the pseudospins is associated with a maximized $K/J$ ratio for the intersite magnetic interactions, through a vanishingly small value of the nearest-neighbor Heisenberg $J$. The apparent correlation between these two features—neat $j_{\text{eff}} = 1/2$ moments and maximized $K/J$ ratio—deserves careful further investigation; for instance, clarifying how different (super)exchange mechanisms cancel out each other for degenerate $t_{2g}$ orbitals but yet distorted metal-ligand-metal paths, when it comes to nearest-neighbor Heisenberg exchange.

*Acknowledgments.* P.B. and L.H. acknowledge financial support from the German Research Foundation (Deutsche Forschungsgemeinschaft, DFG), Project No. 441216021, and technical assistance from U. Nitzsche. S.N., Q.S., and J.G acknowledge financial support through SFB 1143 of the DFG (Project No. 247310070). Q.S. and J.G. thank the Würzburg-Dresden Cluster of Excellence on Complexity and Topology in Quantum Matter (ct.qmat EXC-2147, Project No. 390858490) for financial support. We thank U. K. Rößler for discussions.

[1] A. Kitaev, Ann. Phys. **321**, 2 (2006).
[2] G. Jackeli and G. Khaliullin, Phys. Rev. Lett. **102**, 017205 (2009).
[3] J. Chaloupka, G. Jackeli, and G. Khaliullin, Phys. Rev. Lett. **105**, 027204 (2010).
[4] H.-C. Jiang, Z.-C. Gu, X.-L. Qi, and S. Trebst, Phys. Rev. B **83**, 245104 (2011).
[5] Q. Stahl, T. Ritschel, G. Garbarino, F. Cova, A. Isaeva, T. Doert, and J. Geck, arXiv:2209.08367.
[6] A. Banerjee, C. A. Bridges, J.-Q. Yan, A. A. Aczel, L. Li, M. B. Stone, G. E. Granroth, M. D. Lumsden, Y. Yiu, J. Knolle, S. Bhattacharjee, D. L. Kovrizhin, R. Moessner, D. A. Tennant, D. G. Mandrus, and S. E. Nagler, Nat. Mater. **15**, 733 (2016).
[7] S.-H. Baek, S.-H. Do, K.-Y. Choi, Y. S. Kwon, A. U. B. Wolter, S. Nishimoto, J. van den Brink, and B. Büchner, Phys. Rev. Lett. **119**, 037201 (2017).
[8] Z. Wang, S. Reschke, D. Hüvonen, S.-H. Do, K.-Y. Choi, M. Gensch, U. Nagel, T. Rõõm, and A. Loidl, Phys. Rev. Lett. **119**, 227202 (2017).
[9] J. Zheng, K. Ran, T. Li, J. Wang, P. Wang, B. Liu, Z.-X. Liu, B. Normand, J. Wen, and W. Yu, Phys. Rev. Lett. **119**, 227208 (2017).
[10] R. Yadav, N. A. Bogdanov, V. M. Katukuri, S. Nishimoto, J. van den Brink, and L. Hozoi, Sci. Rep. **6**, 37925 (2016).
[11] S. M. Winter, Y. Li, H. O. Jeschke, and R. Valentí, Phys. Rev. B **93**, 214431 (2016).

[12] P. Warzanowski, N. Borgwardt, K. Hopfer, J. Attig, T. C. Koethe, P. Becker, V. Tsurkan, A. Loidl, M. Hermanns, P. H. M. van Loosdrecht, and M. Grüninger, Phys. Rev. Res. **2**, 042007(R) (2020).
[13] B. W. Lebert, S. Kim, V. Bisogni, I. Jarrige, A. M. Barbour, and Y.-J. Kim, J. Phys.: Condens. Matter **32**, 144001 (2020).
[14] A. Abragam and B. Bleaney, *Electron Paramagnetic Resonance of Transition Ions* (Clarendon Press, Oxford, 1970).
[15] H.-J. Werner, P. J. Knowles, G. Knizia, F. R. Manby, and M. Schütz, WIREs Comput. Mol. Sci **2**, 242 (2012).
[16] See Supplemental Material at http://link.aps.org/supplemental/10.1103/PhysRevB.108.L161107 for basis set details and exact diagonalization calculations. The Supplemental Material also contains Refs. [35–40].
[17] M. Klintenberg, S. Derenzo, and M. Weber, Comput. Phys. Commun. **131**, 120 (2000).
[18] S. E. Derenzo, M. K. Klintenberg, and M. J. Weber, J. Chem. Phys. **112**, 2074 (2000).
[19] T. Helgaker, P. Jørgensen, and J. Olsen, *Molecular Electronic Structure Theory* (Wiley, Chichester, 2000).
[20] D. A. Kreplin, P. J. Knowles, and H.-J. Werner, J. Chem. Phys. **152**, 074102 (2020).
[21] P. J. Knowles and H.-J. Werner, Theor. Chim. Acta **84**, 95 (1992).
[22] A. Berning, M. Schweizer, H.-J. Werner, P. J. Knowles, and P. Palmieri, Mol. Phys. **98**, 1823 (2000).
[23] N. A. Bogdanov, V. M. Katukuri, J. Romhányi, V. Yushankhai, V. Kataev, B. Büchner, J. van den Brink, and L. Hozoi, Nat. Commun. **6**, 7306 (2015).
[24] S. Nishimoto, V. M. Katukuri, V. Yushankhai, H. Stoll, U. K. Rößler, L. Hozoi, I. Rousochatzakis, and J. van den Brink, Nat. Commun. **7**, 10273 (2016).
[25] P. Bhattacharyya, N. A. Bogdanov, S. Nishimoto, S. D. Wilson, and L. Hozoi, npj Quantum Mater. **8**, 52 (2023).
[26] N. A. Bogdanov, R. Maurice, I. Rousochatzakis, J. van den Brink, and L. Hozoi, Phys. Rev. Lett. **110**, 127206 (2013).
[27] R. Yadav, M. S. Eldeeb, R. Ray, S. Aswartham, M. I. Sturza, S. Nishimoto, J. van den Brink, and L. Hozoi, Chem. Sci. **10**, 1866 (2019).
[28] A. Banerjee, J. Yan, J. Knolle, C. A. Bridges, M. B. Stone, M. D. Lumsden, D. G. Mandrus, D. A. Tennant, R. Moessner, and S. E. Nagler, Science **356**, 1055 (2017).
[29] S. M. Winter, K. Riedl, P. A. Maksimov, A. L. Chernyshev, A. Honecker, and R. Valentí, Nat. Commun. **8**, 1152 (2017).
[30] A. Revelli, C. C. Loo, D. Kiese, P. Becker, T. Fröhlich, T. Lorenz, M. Moretti Sala, G. Monaco, F. L. Buessen, J. Attig, M. Hermanns, S. V. Streltsov, D. I. Khomskii, J. van den Brink, M. Braden, P. H. M. van Loosdrecht, S. Trebst, A. Paramekanti, and M. Grüninger, Phys. Rev. B **100**, 085139 (2019).
[31] D. Reig-i-Plessis, T. A. Johnson, K. Lu, Q. Chen, J. P. C. Ruff, M. H. Upton, T. J. Williams, S. Calder, H. D. Zhou, J. P. Clancy, A. A. Aczel, and G. J. MacDougall, Phys. Rev. Mater. **4**, 124407 (2020).
[32] N. Khan, D. Prishchenko, M. H. Upton, V. G. Mazurenko, and A. A. Tsirlin, Phys. Rev. B **103**, 125158 (2021).
[33] M. van Veenendaal, E. H. T. Poldi, L. S. I. Veiga, P. Bencok, G. Fabbris, R. Tartaglia, J. L. McChesney, J. W. Freeland, R. J. Hemley, H. Zheng, J. F. Mitchell, J.-Q. Yan, and D. Haskel, Phys. Rev. B **107**, 214443 (2023).
[34] T. Petersen, L. Prodan, K. Geirhos, H. Nakamura, I. Kézsmárki, and L. Hozoi, Sci. Rep. **13**, 2411 (2023).
[35] P. Fuentealba, H. Preuss, H. Stoll, and L. Von Szentpály, Chem. Phys. Lett. **89**, 418 (1982).
[36] K. A. Peterson, D. Figgen, M. Dolg, and H. Stoll, J. Chem. Phys. **126**, 124101 (2007).
[37] D. Figgen, K. A. Peterson, M. Dolg, and H. Stoll, J. Chem. Phys. **130**, 164108 (2009).
[38] T. H. Dunning, J. Chem. Phys. **90**, 1007 (1989).
[39] D. E. Woon and T. H. Dunning, Jr., J. Chem. Phys. **98**, 1358 (1993).
[40] K. Pierloot, B. Dumez, P.-O. Widmark, and B. O. Roos, Theor. Chim. Acta **90**, 87 (1995).